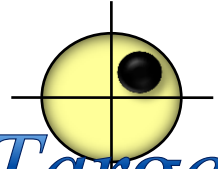


Target Exploration

Energy Geosciences Research & Development

Bapp



Target



**Stratigraphy, Seismic Anomalies
& Typical Fields of Sabratalah Basin**

Offshore Libya

Target Exploration Report Tar150

THE REPORT

The Sabratah Basin of western offshore Libya extends into onshore Tunisia is exhibiting ideal conditions for hydrocarbon generation, migration and accumulation. The lower Eocene Nummulitic carbonate reservoirs hitherto formed the main producing reservoirs and exploration targets in both countries.

This study discovered that wells and outcrop controls indicates that the late Mesozoic and Cenozoic periods at the Sabratah Basin accommodated high energy carbonates, along its flank which are grading into deeper water limestone and fine clastic source rocks towards its centre.

The main structure forming mechanism is provided by the interaction of listric growth and transpressional faults with the Upper Triassic to Lower Jurassic evaporites, which are thick enough to form the salt structures and salt diapirs, such as the salt cored anticline of the Giant Bouri Oil Field.

The Report is a result of extensive of study of the tectonics history and seismic mapping of petroleum geology of Sabratah Basin. The report contains tables of formation tops, seismic sections and other data used in the study with comprehensive references list.

TABLE OF CONTENTS

NO.	CHAPTERS AND SECTIONS	PAGE
I	EXECUTIVE SUMMARY	I
II	TABLE OF CONTENTS V	V
III	LIST OF FIGURES IX	IX
IV	LIST OF TABLES	XVII
V	APPENDICES	XXVII
CHAPTER 1	INTRODUCTION	1
1.1	1.1 General Background 1	1
1.2	1.2 Oil Exploration Activity in the Study Area 3	3

1.3	1.3 Aims and Approach	4
1.4	1.4 Structure of Report	6
CHAPTER 2	BACKGROUND GEOLOGY OF THE MEDITERRANEAN REGION AND PELAGIA	8
2.1	2.1 Introduction	8
2.2	2.2 Tectonic setting of the Mediterranean Region	8
2.3	2.3 Tectonic Setting of the Pelagian Domain and Sabratah Basin	17
	2.3.1 Introduction	17
	2.3.2 Regional Tectonic Setting of the Pelagia	17
	2.3.3 Sabratah Basin	23
	2.4 Bathymetry	24
	2.5 Magmatism in the Pelagia and surrounding region	24
CHAPTER 3	STRATIGRAPHY OF SABRATAH BASIN	34
3.1	Introduction:	34
	3.2 TRIASSIC SEQUENCE	40
	3.2.1 AL Guidr Formation (Lower Triassic)	41
	3.2.2 Kurrush Formation (Middle Triassic)	42
	3.2.3 Al Azizyah Formation (Middle-Upper Triassic)	42
	3.2.4 Abu Shaybah Formation (Late Triassic-Early Jurassic)	43
	3.3 JURASSIC SEQUENCE	46
	3.3.1 Bir-Al Ghanam Formation (Lower-Mid Jurassic)	46
	3.3.2 Kiklah formation (Middle -Jurassic –Early Cretaceous)	47
	3.4 CRETACEOUS SEQUENCE	48
	3.4.1 Alalgah Formation (Cenomanian)	49
	3.4.2 Makhbaz Formation (Turonian- Coniacian)	49
	3.4.3 Jamil Formation (Santonian)	50
	3.4.4 Bu Isa Formation (Campanian)	51
	3.4.5 Al Jurf Formation (Maastrichtian- Paleocene)	51
	3.5 PALEOCENE SEQUENCE	52
	3.6 EOCENE SEQUENCE	53
	3.6.1 Bilal Formation (Late Landenian-Early Ypresian)	54
	3.6.2 Jirani Dolomite (Ypresian)	55
	3.6.3 Jdeir formation (Late Ypresian –Early Lutetian)	55

	3.6.4 Harshah Formation (Lutetian)	55	55
	3.6.5 Dahman Formation (Late Lutetian-Early Priabonian)	56	56
	3.6.6 Samdun Formation (Base Oligocene)	58	58
	3.7 OLIGOCENE SEQUENCE	58	58
	3.7.1 Ras Abd Jalil Formation (Oligocene Early Miocene)	59	59
	3.7.2 Dirbal Formation (Oligocene Early Miocene)	60	60
	3.8 MIOCENE SEQUENCE	60	60
	3.8.1 Ain Grab Formation (Burdigalian)	61	61
	3.8.2 Al Mayah Formation (Middle Miocene)	61	61
	3.8.3 Tubtah Formation (Middle - Upper Miocene)	62	62
	3.8.4 Marsa Zouaghah Formation (Messinian)	62	62
CHAPTER 4	STRUCTURAL INTERPRETATION	64	64
4.1	Seismic data	64	64
	4.2 Mis-tie correction	64	64
	4.3 Synthetic Seismograms	68	68
	4.4 Picked horizons and isochrones maps	69	69
	4.4.1 Seabed horizon	69	69
	4.4.2 Top Tubtah	73	73
	4.4.3 Top Ain Grab	79	79
	4.4.4 Top Samdun (Base Oligocene)	79	79
	4.4.5 Top Jdeir (Lower Eocene)	84	84
	4.4.6 Top Lower Al Jurf (Basal Tertiary)	84	84
	4.4.7 Top Makhbaz (Turonian- Coniacian)	88	88
	4.4.8 Bir Al Ghanam (Lower - Middle Jurassic)	94	94
	4.5 Structure Interpretation of Area A	98	98
	4.5.1 Introduction	98	98
	4.5.2 Periclinal folding and faulting	99	99
	4.5.3 Timing and geodynamic setting of share	101	101
	4.5.4 Topographic inversion (Alpine tectonic cycles)	106	106
	4.6 Structure interpretation of Area B	110	110
	4.6.1 Introduction	110	110
	4.6.2 Planar and listric faults	113	113

	4.6.3 Salt Tectonics In Area B	114	114
	4.7 Summary	125	125
CHAPTER 5	SUBSIDENCE HISTORY OF SABRATAH BASIN	127	127
5.1	Introduction	127	127
	5.2 Geo-history Analysis	128	128
	5.2.1 De-compaction	128	128
	5.2.2 Paleo-water depth	129	129
	5.2.3 Eustatic Corrections	130	130
	5.3 1D Back-stripping using Airy isostasy	130	130
	5.3.1 Analysis of basement subsidence curves	132	132
	5.3.2 Investigate the onset of rifting	152	152
	5.4 Estimation of the stretching factor (β) and Thinning factor	166	166
	5.5 Summary	181	181
CHAPTER 6	INTERPRETATION OF THE GRAVITY AND MAGNETIC DATA		183
6.1	Introduction	183	183
	6.2 Interpretation of Gravity data	184	184
	6.2.1 Gravity dataset	184	184
	6.2.2 Regional-Residual Field Separation	186	186
	6.2.3 Boundary analysis techniques	199	199
	6.3 Interpretation of Magnetic Data	214	214
	6.3.1 Introduction	214	214
	6.3.2 Magnetic dataset	214	214
	6.3.3 Reduction to the pole and pseudo-gravity transforms	217	217
	6.3.4 Spectral analysis and Filtering	219	219
	6.3.5 Edge Detection of Magnetic Sources	226	226
	6.3.6 Depth to magnetic sources	231	231
	6.4 Generalized interpretation map	234	234
	6.5 Forward Modelling	234	234
	6.6 Summary	243	243
CHAPTER 7	CONCLUSIONS AND RECOMMENDED FUTURE WORK	245	245
7.1	Introduction	245	245
	7.2 Crustal structure and basin formation	245	245

	7.3 Shear between Africa and Europe	250	250
	7.4 Recommended Future Work	255	255
8	LIST OF FIGURES		1X
Figure 1 1:	Structural and tectonics elements map for Libya and adjacent	2	2
	Figure 1 2: Concessions map of the Sabratah Basin. (Base map curtesy of Libyan NOC	5	5
	Figure 2 1 Physiographic provinces for the Mediterranean Sea from.Platt (2007)	9	9
	Figure 2 2: Middle Jurassic Paleo-tectonic map of Arabia and North Africa (de Lamotte et al., 2011)	11	11
	Figure 2 3 Trajectories of three points in Africa relative to fixed points in Europe from (Rosenbaum et al., 2002b)	14	14
	Figure 2 4. Location of the rollback process in the Mediterranean Sea	16	16
	Figure 2 5: A Reconstruction of the Hercynian, showing the WNW fault in the Libyan offshore were developed as part of a right-lateral mega-shear zone. From (Dewey and Booth, 1988)	19	19
	Figure 2 6 Structural sketch map of the South Tethys margin (present state) from (Frizon de Lamotte et al., 2011)	20	20
	Figure 2 7: The reversal of strike slip motion along the Hercynian fault system would cause Sabratah Basin, the Libyan Coastal fault system were part of the WNW trending faults of Pelagia. From (Dewey and Booth, 1988)	21	21
	Figure 2 8 Tectonic and morphologic elements of the Pelagian Domain	26	26
	Figure 2 9: Bathymetry of the central and western offshore Libya	27	27
	Figure 2 10: The main extensional phases and relative igneous activity in pelagian and Ionian sea, from Finetti (1982).	30	30
	Figure 2 11 Total magnetic Intensity map of Western and Central offshore Libya	32	32
	Figure 2 12: The Koms magnetic anomaly (M4)	33	33
	Figure 3 1: Stratigraphic correlation chart of geological formations of NW offshore Libya. Modified from (Hammuda et al., 1985; Sbeta, 1990; Rusk, 2001)	35	35
	Figure 3 2: Wells location map from (Hammuda et al., 1985)	36	36
	Figure 3 3: Correlation Chart of Mesozoic and Cenozoic rocks in NW Libya from (Hammuda et al., 1985).	37	37
	Figure 3 4: Location map of cross sections (A-A"), ((B-B") and (C-C)	38	38
	Figure 3 5: Cross section A-A	39	39
	Figure 3 6: Thickness of Triassic formations	41	41
	Figure 3 7: Cross section (B-B")	44	44
	Figure 3 8: Cross section (C-C")	45	45
	Figure 3 9: Thickness of formations of upper Cretaceous rocks	50	50
	Figure 3 10: Thickness of Paleocene rocks	53	53
	Figure 3 11: Thickness of Farwah group in penetrated wells	56	56

Figure 3 12: Distribution of Jdeir formation includes dolomite	57	57
Figure 3 13: Thickness of Tellil group	58	58
Figure 3 14: Thickness of Ras Abd Jalil / Dirbal formations	61	61
Figure 3 15: Thickness of middle upper Miocene	63	63
Figure 4 1: Location map of 3D seismic cubes and 2D seismic profiles	65	65
Figure 4 2: Mis-tie correction between 3D-seismic surveys of concession NC41 (Bouri field) and concession 137N .a) before correction b) after correction	67	67
Figure 4 3: Interpreted seismic profile (202). Location shown in Figure 4 1	70	70
Figure 4 4: Interpreted seismic profile (206). Location shown in Figure 4 1	71	71
Figure 4 5: Interpreted seismic profile (208). Location shown in Figure 4 1	72	72
Figure 4 6: Time structure map of the sea floor. a) For whole study area. b) For the area A. c) For the area B. Scale may not be the same	74	74
Figure 4 7: a) Inline crossing the circular structure in Bouri field. b) Same line showing the structure in details.	75	75
Figure 4 8: interpreted arbitrary Seismic profile trending W-E along the concession 137N and Bouri filed. Location is shown in ?	76	76
Figure 4 9: Time structure map for top Tubtah. a) for whole study area. b) For area A. c) For area B. Scale may not be the same for all maps	77	77
Figure 4 10: Time thickness map (TTM1) between upper Miocene and sea floor. a) Whole study area. b) For area A. c) For area B. Scale may not be the same for all maps	78	78
Figure 4 11: Time structure map for top Ain Grab a) for whole study area. b) For area A. c) For area B. Scale may not be the same for all maps	80	80
Figure 4 12: showing the N60° faults. a) Time slice at 1.5 s for area A. b) Coherency at 1.5 s for concession 137N	82	82
Figure 4 13: The time thickness map (TTM2) between the top Tubtah and top Ain Grab. a) For whole study area. b) For area A. c) For area B.	83	83
Figure 4 14: Time structure map for base Oligocene a) for whole study area. b) For area A. c) For area B. Scale may not be the same	85	85
Figure 4 15: The time thickness map (TTM3) between the Ain Grab and the Samdun Formations.	86	86
Figure 4 16: Time structure map for top of the Jdeir formation.	87	87
Figure 4 17: Interpreted Crossline of Bouri field showing faults within the Farwah group. Location shown in Figure 4 17	89	89
Figure 4 18: The time thickness map (TTM4) between top Samdun and top Jdeir formations.	90	90
Figure 4 19: Interpreted Inline 4989 trending W-E in area B showing the base Tertiary unconformity.	91	91
Figure 4 20: The time structure map of base Tertiary. a) For the whole study area. b) For area A. c) For area B. Scale may not	92	92

be the same	92	
Figure 4 21: The time thickness map (TTM5) between top Jdeir and top of lower Al Jurf formations)	93	93
Figure 4 22: The time structure map of top Makhbaz formation. a) For the whole study area. b) For area B. Scale may not be the same	95	95
Figure 4 23: Time thickness map (TTM6) between the base Tertiary and top Makhbaz	96	96
Figure 4 24: Time structure map of top Bir Al Ghanam Formation	97	97
Figure 4 25: The nine tectonic phases of post Hercynian time, corresponds to changes in motion between Africa and Europe plates. From (Dewey and Booth, 1988)	99	99
Figure 4 26: Plate Tectonic Reconstruction (Campanian) 80 Ma. From (Hallett, 2002)	100	100
Figure 4 27: Interpretation of Periclinal folding and faulting on time structure map of Top Jdeir formation	102	102
Figure 4 28: Seismic line crossing the fold Al Jurf (B) trending NS showing the interpreted Horizons from sea floor to Base Tertiary. Location is shown on Figure 4 27	104	104
Figure 4 29: Seismic line crossing the fold (D) trending NS showing	105	105
Figure 4 30: Seismic line crossing the fold Bouri trending SN showing the interpreted horizons from sea floor to Base Tertiary. Location is shown in	106	106
Figure 4 31: Two Alpine tectonic cycles, first cycle between Base Tertiary and Lower Eocene and second cycle between Lower Miocene and Upper Miocene.	109	109
Figure 4 32: Base map for block B showing the location of displayed seismic lines and the location of salt diapirs.	111	111
Figure 4 33: Interpreted arbitrary seismic line between wells K1-137 offshore side and A1-9 onshore side.	112	112
Figure 4 34: Interpreted Xline 4787, showing the flat-ramp listric	115	115
Figure 4 35: The seismic section in depth showing the same line in Figure 4 34	116	116
Figure 4 36: Seismic section showing a listric fault geometries in the eastern end of area b. location is shown in Figure 4 32	117	117
Figure 4 37: The three stages in the evolution of a salt diapir in the extensional domain. From (Vendeville and Jackson, 1992a).	120	120
Figure 4 38: Highlight the development of salt structure in the NW corner of block b. a) Upper Miocene.	121	121
Figure 4 39: Crossline 1223 trending SN showing salt diapir.	122	122
Figure 4 40: Arbitrary seismic line trending NW-SE crossing two salt structures. Location is shown in Figure 4 32	123	123
Figure 4 41: Interpreted crossline 3320 Trending S-N showing the thin-skinned deformation. Location is shown in Figure 4 32	124	124
Figure 5 1: Lithospheric stretching and subsidence of McKenzie (1978) model.	133	133
Figure 5 2: Wells location and seismic data used for calculating tectonic subsidence.	134	134
Figure 5 3: Decompact Burial History of data shown in Table 5 3 for well L1-137.	139	139

Figure 5 4: Tectonic subsidence curves for 20 wells in Sabratak basin correcting for paleowater depth. Blue line represents minimum tectonic subsidence and red line represents maximum tectonic subsidence	144	144
Figure 5 5: Tectonic subsidence curves for 20 wells in Sabratak basin without paleowater correction.	147	147
Figure 5 6: Seismic line 203 used to extend the wells F1-137, D3137 and S1-NC41 to the Base Jurassic	154	154
Figure 5 7: extended timing of eight wells with consideration of Paleowater. Blue line represents minimum tectonic subsidence and red line represents maximum tectonic subsidence	155	155
Figure 5 8: extended timing of eight wells with ignoring of Paleowater	156	156
Figure 5 9: comparison between tectonic subsidence curves from different locations in the basin. Blue line represents minimum tectonic subsidence and red line represents maximum tectonic subsidence	157	157
Figure 5 10: Tectonic subsidence curve for well L1-137 with compensation of missing sections	158	158
Figure 5 11: Basement subsidence maps; (a) between 70-65 Ma and (b) between 65-56 Ma	159	159
Figure 5 12: Basement subsidence maps; (a) between 56-48 Ma (b) between 48-34 mMa	160	160
Figure 5 13: Basement subsidence maps; (a) between 34-17 mMa and (b) between 17-12 Ma	161	161
Figure 5 14: Basement subsidence maps; (a) between 12-7 Ma and (b) between 7-5 Ma (c) between 5-0 Ma	162	162
Figure 5 15: Extending the initial rift of the basin using the information from seismic data. Blue line represents minimum tectonic subsidence and red line represents maximum tectonic subsidence	165	165
Figure 5 16: Tectonic subsidence plot for wells L1-137, H1-NC41 and S1-NC41 showing the onset of two rift events.	167	167
Figure 5 17: Deep seismic line R01 from (Faux et al., 1988)	169	169
Figure 5 18: Geometry of the Airy- Heiskanen compensation model	170	170
Figure 5 19: Depth to the Moho for depth of sea level compensation 35km	172	172
Figure 5 20: Depth to basement (a) in time sec. (b) depth in meter	173	173
Figure 5 21: Thickness of the basement obtained by subtracting the depth to the basement from depth to the Moho	174	174
Figure 5 22: Stretching factor for the Sabratak Basin obtained by divided the initial crustal thickness (35km) by the thickness of the basement	175	175
Figure 5 23: Thinning factor for the Sabratak Basin for initial crustal thickness 35km	177	177
Figure 5 24: Thickness of the basement obtained by using the Warner (1987) method assuming the time depth to the Moho; (a) 10 s (b) 11s.	178	178
Figure 5 25: Stretching factor for the Sabratak Basin obtained by divided initial crustal thickness (35km)	179	179
Figure 6 1: Bouguer gravity map for the central and NW offshore Libya. The map was gridded using 2km x2km grid cell size		188
Figure 6 2: (a) distribution of the gravity stations (b) Simple Bouguer gravity map created using 1km x 1km grid cell size		189
Figure 6 3: (a) Depth to the Moho map for west and central offshore Libya, depth of sea level compensation set to 35km (b)The		190

3D gravity response of the root (isostatic regional gravity field)	190	
Figure 6 4: isostatic residual anomaly of the study area	191	191
Figure 6 5(a) Radially averaged power spectrum (b) low pass wavelength 100km (c) high pass wavelength 100km (d) 100-28km bandwidth	194	194
Figure 6 6: Residual gravity fields obtained from fitting polynomial trend to Bouguer gravity (a) 1st order (b) 2nd order (c) 3rd order	195	195
Figure 6 7: Polynomial trend surfaces (a)1st order (b) 2nd order (c) 3rd order	196	196
Figure 6 8: Upward continuation (a) up to 7km (b) up to 13 km	200	200
Figure 6 9: Separation filter (a) difference between upward continuations 13km-7km (b) difference between upward continuations 60km-20km	201	201
Figure 6 10 North–south structural cross-section across the Sabratah and Ghadamis Basins study area highlighted, from Bodin et al. (2010)	202	202
Figure 6 11: Analytic signal map of 3rd order residual of gravity data	204	204
Figure 6 12: (a) Total horizontal gradient map of 3rd order residual of gravity	209	209
Figure 6 13: (a) First Vertical gradient of-3rd order residual gravity field (b) Tilt angle of 3rd order residual gravity	210	210
Figure 6 14: Comparison between Bouguer gravity and its tilt angle with seismic data along NS profile crossing well K1-137	211	211
Figure 6 15: Comparison between gravity, magnetic and seismic data along NW-SE profile	212	212
Figure 6 16: Comparison between Bouguer gravity and its tilt angle with seismic data along SN profile crossing salt diaper	213	213
Figure 6 17: (a) Distribution of magnetic field observation points (b) Total magnetic intensity map of the study	216	216
Figure 6 18: (a) Reduction to the north magnetic pole map for induced magnetization at the present day field ($D=0^\circ$, $I=47^\circ$) (b) pseudogravity field for induced magnetization at the present day field ($D=0^\circ$, $I=47^\circ$) and a ratio of intensity of magnetization to density contrast of unity.	220	220
Figure 6 19: Comparison of pseudogravity field (contours mGal) with Bouguer gravity map for induced magnetization at the present day field ($D=0^\circ$, $I=47^\circ$).	221	221
Figure 6 20: (a) Power spectrum plot for Reduced to pole total magnetic field. (b) Radial spectrum plot of the magnetic Reduction to the pole	223	223
Figure 6 21: Geothermal gradient map the study area	225	225
Figure 6 22: Low pass cut off 5.8km of Reduced to pole total magnetic field (RTP)	227	227
Figure 6 23: Source edge detection (a) location of maxima of total horizontal gradient	230	230
Figure 6 24: Euler's depth estimates (5-16km). Reduction to the north magnetic pole shown in the Background	233	233
Figure 6 25: Generalized interpretation map of the gravity and magnetic data	235	235

	Figure 6 26: The location of the models AA' and BB' are shown on Bouguer gravity map gridded 1km x 1km	239
	Figure 6 27: 2D gravity model performed along profile AA'. Observed and calculated Bouguer gravity anomalies are black dotted and brown solid lines. Location of the model is shown in Figure 6 26	240
	Figure 6 28:Arbitaray seismic line along model profile BB'.	241
	Figure 6 29: the2D gravity and magnetic model performed along profile BB', location shown in	242
	Figure 7 1: Geological cross section between the southern part of Sabratah Basin and Ghadamis Basin crossing the Jeffara region. From(Swire, 2000)	247
	Figure 7 2: Geological cross section from Bouri Oil Field to onshore region, showing the displacement due to Libyan Coastal Fault System. Modified from (Sbeta, 1991)	248
	Figure 7 3: Dextral strike slip movement along Libyan Coastal Fault System and Cyrenaica Coastal Fault System, showing the relationship between Sabratah- Cyrenaica Coastal Fault System, Sirt rift complex and Tiji-Nalut Fault Zone. After (Anketell and Ghellali, 1991;Anketell, 1996)	251
	Figure 7 4: Map showing the different structures within the area A and B including Oil and Gas fields	253
9	LIST OF TABLES	XVII
Table 2- 1:	Volcanic occurrences in the study area	31
	Table 5 -1: Thickness of 15 stratigraphic units at present day in compacted state	135
	Table 5 -2: The de-compacted thickness versus age for 15 stratigraphic units.	136
	Table 5 3: The decompacted depth versus age for 15 stratigraphic units.	137
	Table 5 -4: Tectonic subsidence data for well L1-137	138
	Table 5 -5 showing stretching factor from different sources	180
	Table 6 -1: Type and time of the gravity surveys in the study area	185
	Table 6 -2. Calibrated Geothermal Gradient data for wells in the study area	224
	Table 6 -3: Density data calculated from well log and used for model AA'	238
	Table 7 -1: Diapiric structures distribution and their ages in the Mediterranean Sea.	255
10	APPENDICES	XXVII
Appendix A:	Palaeobathymetry estimated based on various well information	ii
Appendix B:	formation tops, thickness, lithology and paleo-water depth	iii



This report is available for immediate dispatch from

Target Exploration Consultants

[Click here to purchase your copy](#)

For further information, contact:

M. Casey,

Target Exploration

65 Kenton Court, London W14 8NW, UK.

target@targetexploration.com

www.targetexploration.com

[Home](#)

[About Us](#)

[Experience](#)

[Services](#)

[Training](#)

[Conferences](#)

[Publications](#)

[Order Form](#)

[News](#)

[Careers](#)

[Contracts](#)

[Downloads](#)

[Uploads](#)

[Links](#)

[Rep/Software](#)

[Contact Us](#)



[22-02-2022](#)